Effects of the asymmetric and oscillating turbulent melt flow on the heat transfer and solidification inside the thin slab continuous casting (TSC) mold under the applied electromagnetic brake (EMBr)

Journal of Physics: Conference Series **2766** (2024) 012196 doi:10.1088/1742-6596/2766/1/012196

Effects of the asymmetric and oscillating turbulent melt flow on the heat transfer and solidification inside the thin slab continuous casting (TSC) mold under the applied electromagnetic brake (EMBr)

A Vakhrushev[1], E Karimi-Sibaki[1], M Wu[2], Y Tang[3], G Hackl[3], J Watzinger[4], J Bohacek[5] and A Kharicha[1]

[1]Christian-Doppler Lab for Metallurgical Applications of Magnetohydrodynamics, University of Leoben, Franz-Josef-Str. 18, 8700 Leoben, Austria
[2]Chair of Simulation and Modeling of Metallurgical Processes, University of Leoben, Franz-Josef-Str. 18, 8700 Leoben, Austria
[3]RHI Magnesita GmbH, Technolgy Centre, Magnesitstrasse 2, 8700, Leoben, Austria
[4]Primetals Technologies, Turmstrasse 44, 4031, Linz, Austria
[5]Heat Transfer and Fluid Flow Laboratory, Faculty of Mechanical Engineering, Brno University of Technology, 61669 Brno, Czech Republic

E-mail: abdellah.kharicha@unileoben.ac.at

Abstract. The thin slab casting (TSC) is a breakthrough near-net-shape technique for flat products accompanied by rapid casting and solidification rates. The TSC quality hinges on the turbulence, super-heat flow and growth of the solidified shell. The electromagnetic brake (EMBr) is commonly applied to control the fresh melt flow after feeding through a submerged entry nozzle (SEN). Numerical modelling is a perfect tool to investigate the multiphase phenomena in the continuous casting (CC). The presented study considers the heat transfer through the solid shell and water-cooled copper mold including the averaged thermal resistance of the slag skin and the air gap coupled with the turbulent flow and magnetohydrodynamics (MHD) model using an in-house code developed inside the open-source computational fluid dynamics (CFD) package OpenFOAM®. The model is applied to investigate different undesired asymmetric melt flow issues: (i) with the misaligned or (ii) partially blocked SEN; (iii) caused by the mean flow fluctuations with the natural frequencies; (iv) related to the oscillations of the fresh melt jets for the specific SEN designs and casting regimes. The variation of the flow pattern and superheat distribution is studied and presented for different scenarios both with and without applied EMBr.

1. Introduction

The near-net-shape thin slab casting (TSC) is known as a technological breakthrough in the steel industry during the last decades. However, rapid casting is accompanied by an active generation of turbulence inside a funnel type mold. The turbulent jets, after being fed through the submerged entry nozzle (SEN), impact on the mushy zone [1]. The impingement of the hot melt suppresses the growth or even leads to a partial remelting of the solidifying shell, thus, promoting a breakout formation [2,3].

The corresponding liquid pool depth affects the strand's contraction / dilatation under the supporting rolls and impacts solute distribution during the mechanical reduction [4].
The electromagnetic braking (EMBr) was under developed alongside with the casing technologies to become an efficient technique to control the mold flow [5]. The mold flow pattern, superheat distribution and melt solidification are significantly altered under the EMBr during the continuous casting (CC) process [6–11]. As recently revealed, one must bear in mind a complex topology of the Lorentz force in application to CC process. The damping action is accompanied by the formation of the reverse zones in the vicinity of the feeding jets (flattened along direct current (DC) magnetic field) [12] and inside the upper region of the CC mold [13,14], where the MHD flow vastly affects free surface flow [15].

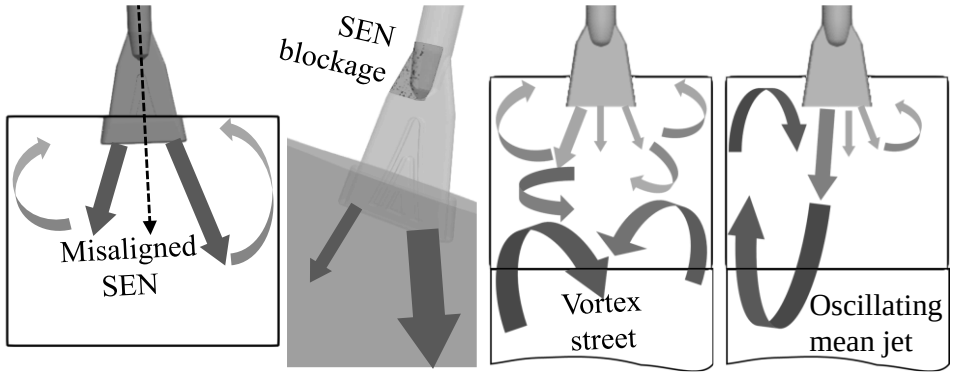

Figure 1. Types of the melt instabilities in the study: asymmetric pattern due to the (a) misalignment or (b) partial SEN blockage; fluctuating flow in form of (c) a vortex street or (d) oscillating mean jet.

The misalignment of the SEN or its clogging during operation are common issues in the CC process causing the jets / mean flow oscillations or / and asymmetry. Different flow instabilities produce high fluctuations of liquid bath and meniscus [16–19]. The presented numerical study examines solidification during the TSC with the asymmetric flow patterns, listed in figure 1, originating from the mechanical sources or due to the transition into the naturally unstable regimes. These effects are considered with and without an applied EMBr by analyzing the changes in velocity and temperature fields.

2. Numerical model

The previously verified approach using volume averaging mixture formulation [20] was used to model velocity $\vec{u}$ of the turbulent melt flow, the solidification and the MHD forces:

$$\rho\left[\frac{\partial\vec{u}}{\partial t}+\nabla\bullet(\vec{u}\otimes\vec{u})\right]=\nabla\bullet\boldsymbol{\sigma}_{\text{eff}}-\nabla p+\vec{F}_{\text{mush}}+\vec{F}_{\text{MHD}}\,, \tag{1}$$

where t, ρ and p are correspondingly the time variable, density and pressure; $\boldsymbol{\sigma}_{\text{eff}}$ is a viscous stress including turbulent effects, which were considered using the wall-adapting local eddy-viscosity (WALE) sub-grid scale (SGS) model [21]; $\vec{F}_{\text{mush}}$ represents the drag from the columnar-type mushy zone [20]; $\vec{F}_{\text{MHD}}$ is the Lorentz force calculated using the conservative formulation by Ni et al. [22] for the electric potential method [23] and implemented inside the in-house MHD code [13,14].
The corresponding energy equation for the temperature field T [20]

$$\rho C_{\text{p}}\left[\frac{\partial T}{\partial t}+\nabla\bullet(\vec{u}T)\right]=\nabla\bullet\lambda\nabla T+\rho L\left[\frac{\partial f_{\text{s}}}{\partial t}+\nabla\bullet(f_{\text{s}}\cdot\vec{u}_{\text{s}})\right] \tag{2}$$

with the specific heat C_{p}, thermal conductivity λ and solid fraction f_{s} regards the distribution of the solid velocities $\vec{u}_{\text{s}}$ following the funnel-shaped mold [20,24,25] to accurately treat advection of the latent heat L [1]. The numerical model employs the OpenFOAM® finite volume method (FVM) framework [26].
The alloy properties, listed in reference [27], are calculated in the thermodynamic software IDS [28]. To summarize them for the readers, a casting velocity of 4.8−5.5 m/min, solidus / liquidus temperatures of 1788.15 K / 1805.15 K and a pouring temperature of 1824.15 K are applied for the presented results.

A mold heat flux is commonly taken from literature, evaluated from the plant measurements or modeled directly [20,24,29,30]. Here, a previously developed heat extraction model including a thermal resistance between the shell and the hot wall of the water cooled TSC mold was used [31]. An effective heat transfer coefficient (HTC) of 1100 W/m^{2}K, obtained by the in-house implementation of the inverse heat conduction problem (IHCP) method [32], defines the secondary cooling zone in the slab region.

3. Simulation results

In this section we firstly consider mechanically-related melt flow issues in the TSC mold, such as caused by the misalignment of the SEN or due to its partial blockage.

The simulation results of the solidification inside the TSC mold with the tilted SEN are in figure 2. The distribution of the velocity (figure 2-a,b) and temperature (figure 2-c,d) fields in the midplane are presented for the no magnetic field and EMBr cases. The corresponding magnetic field distribution is in figure 2-e. Without magnetic field, the jet on the tilting-wise side of the mold goes deeper into the melt pool, whereas on the opposite side the upper roll is close to meniscus (figure 2-a). That results in more superheat on the left side and in formation of a colder region on the right side (figure 2-c).

When the EMBr is applied the flow becomes more symmetric with a slightly slower upper roll on the right in figure 2-b, and the temperature field is leveled as well (see in figure 2-d). Since the application of the symmetric magnetic field itself led to improvements, an adjustable EMBr was employed through the simulation series to find an optimal brake power, which was detailed in a recent study [27].

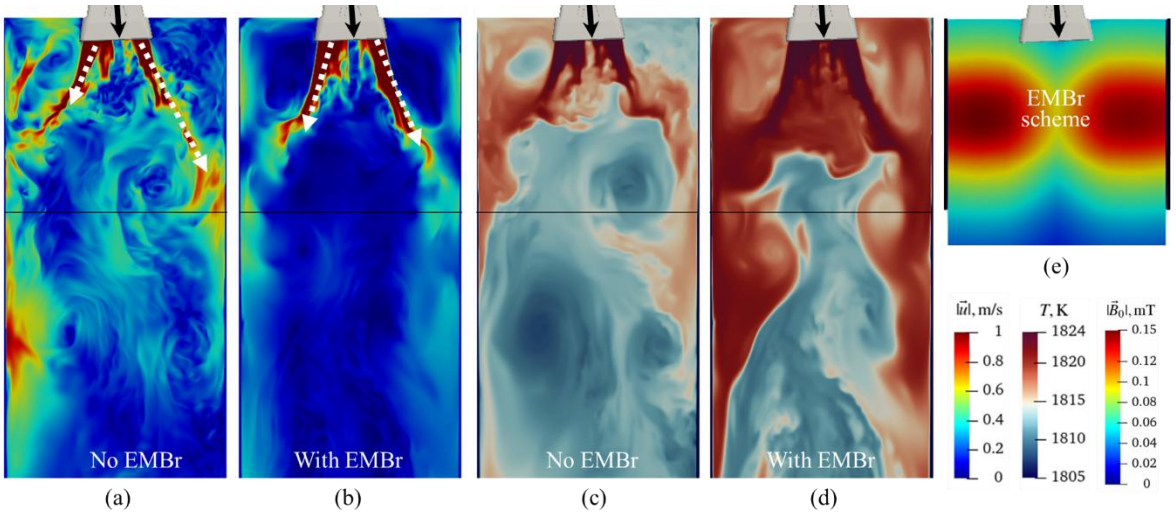

Figure 2. Simulation results for the misaligned by 2° SEN: distribution of the (a)-(b) flow velocity and (c)-(d) temperature field without (left figures) and with applied magnetic field (right figures); (e) EMBr schematics with the applied magnetic field $\vec{B}_0$ and SEN tilting direction.

The influence of the applied magnetic field on the asymmetric flow inside a TSC mold due to the partial SEN blockage was recently presented by the authors including effects on the solidification profiles [33]. The SEN clogging can occur during deposition of the non-metallic inclusions [34] or due to the combined effect with the parasitic solidification inside the SEN bore because of the heat losses [35].

As seen in figure 3-a, an undesired asymmetric flow pattern is formed after the clogging formation inside the SEN bore. The heat transfer issues are clearly detected in figure 3-c. The submeniscus on the right (non-blocked) side is dominantly colder since the fast jet penetrates deeper into the liquid bath. Moreover, due to the side-to-side swinging the temperatures can dangerously drop everywhere along the top surface once the melt flow is fully downward as detailed in figure 7 of reference [33].

Once the EMBr is applied (figure 3-e), the fluctuations are “frozen”: the non-clogged jet impacts on the narrow side shell far below the mold exit, thus, promoting the breakout risks. Despite the corresponding sub-meniscus region becoming stagnant (figure 3-b), more superheat is kept at the top part of a TSC mold due to the braking effects (figure 3-d).

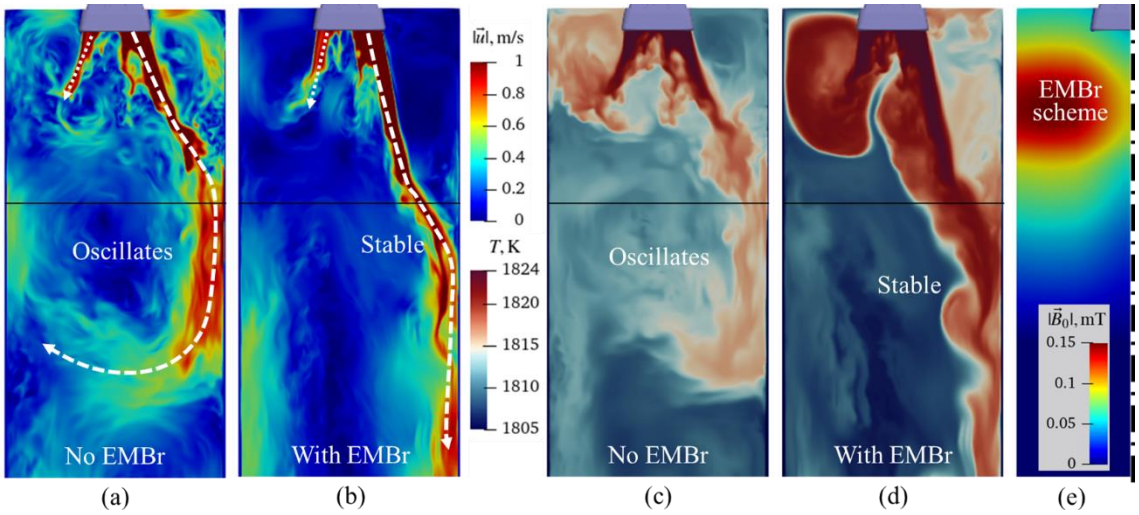

Figure 3. Simulation results for the partially blocked SEN: distribution of the (a)-(b) flow velocity and (c)-(d) temperature field without (left figures) and with applied magnetic field (right figures); (e) EMBr schematics with the applied magnetic field $\vec{B}_0$.

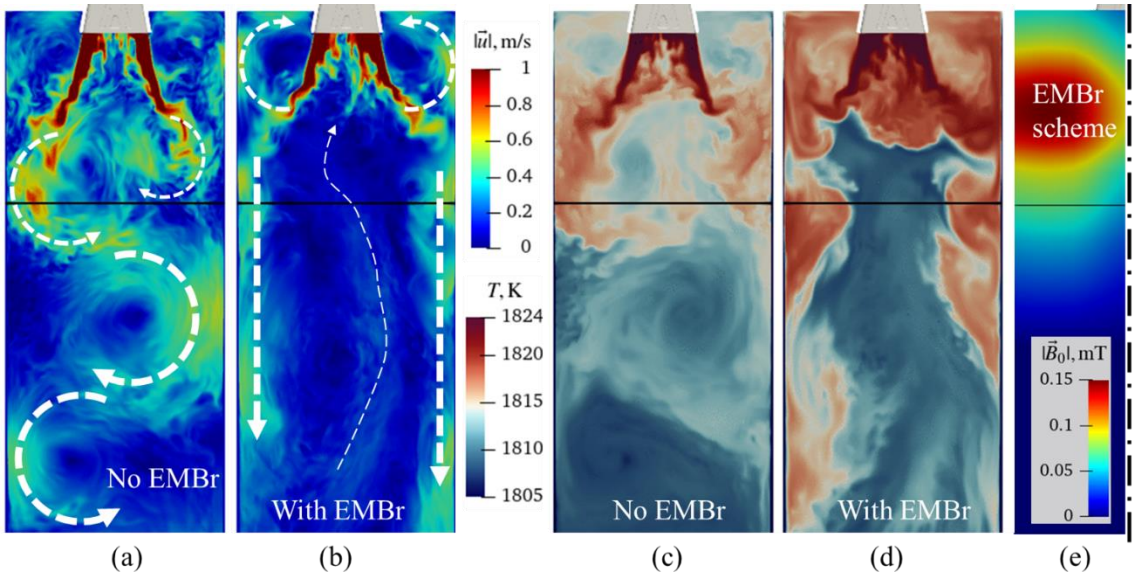

Figure 4. Simulation results for the fluctuating mean flow: distribution of the (a)-(b) flow velocity and (c)-(d) temperature field without (left figures) and with applied magnetic field (right figures); (e) EMBr schematics with the applied magnetic field $\vec{B}_0$.

Figure 4 gathers studies for a flow oscillation regime with the eigen frequencies coming from the formation kind of a vortex street. These coherent structures in figure 4-a are clearly initiated at the jet region and further develop from the mold exit into the slab section. Regarding the superheat in figure 4-c, relatively much mixing happens in the TSC mold. However, some strong local temperature gradients are detected causing non-uniform solidification in the transversal direction. With the applied magnetic field (figure 4-e), the upper rolls are stabilized promoting the superheat transport towards meniscus (figure 4-b). Below the EMBr region, the central flow is reversed into a weak upstream motion (figure 4-b). Most of the hot melt moves along the narrow walls downwards (figure 4-d).
In the case of the oscillating jet (see figure 5-a) a completely asymmetric pattern is observed with a subsequent change of the jet's location between left and right narrow walls. The hydrodynamics of this phenomenon is detailed in a recent study for the 1-to-2 water modelling scale [36].

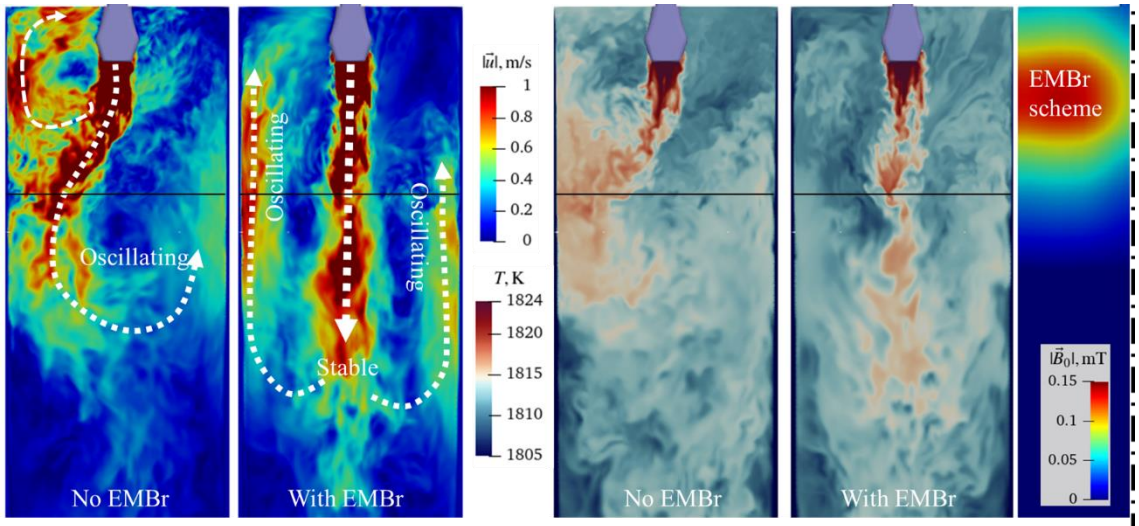

Figure 5. Simulation results for the oscillating jet: distribution of the (a)-(b) flow velocity and (c)-(d) temperature field without (left figures) and with applied magnetic field (right figures); (e) EMBr schematics with the applied magnetic field $\vec{B}_0$.

For the presented industrial case the fluctuations period amounts to 13-15 seconds leading to the corresponding uneven superheat distribution in figure 5-c. However, a jet is stabilized by the DC magnetic field (sketched in figure 5-e) with a slightly upward fluctuating along the narrow walls (see figure 5-b). A fresh melt is transported uniformly under the braking. However, more superheat is brought to the lower part of the mold, and a slightly colder region appears near the meniscus. Thus, one can consider an optimized EMBr scenario with more braking in the middle of the mold.

4. Conclusions

As detailed in this study, the application of the EMBr at the presence of different types of the flow asymmetry and instabilities can both improve the flow pattern and superheat distribution, e.g. in case of the oscillating jet and vortex street formation, as well as worsen the negative consequences and promote the breakout risks, e.g. for the partially blocked SEN. In some scenarios, e.g. with the misaligned by tilting SEN, an adjustable magnetic field must be employed to achieve the best braking strategy.

5. Acknowledgments

The authors acknowledge the financial support by the Austrian Federal Ministry of Economy, Family and Youth and the National Foundation for Research, Technology and Development within the framework of the Christian Doppler Laboratory for Metallurgical Applications of Magnetohydrodynamics.

References

[1] Wu M, Vakhrushev A, Ludwig A and Kharicha A 2016 *IOP Conf. Ser.: Mater. Sci. Eng.* **117** 012045
[2] Iwasaki J and Thomas B G 2012 *Supplemental Proceedings* ed TMS (Wiley) pp 355–62
[3] Zappulla M L S, Cho S and Thomas B G 2019 *Steel Res. Int.* **90** 1800540
[4] Guan R, Rodrigues C M G, Ji C, Zhu M, Li S, Wu M, Kharicha A, Vakhrushev A and Ludwig A 2023 *Appl. Math. Model.* **114** 770–84
[5] Thomas B G and Cho S M 2018 *IOP Conf. Ser.: Mater. Sci. Eng.* **424** 012027
[6] Chaudhary R, Thomas B G and Vanka S P 2012 *Metall. Mater. Trans. B* **43** 532–53
[7] Thomas B G, Singh R, Vanka S P, Timmel K, Eckert S and Gerbeth G 2015 *J. Manuf. Sci. Prod.* **15** 93–104

[8] Vakhrushev A, Kharicha A, Liu Z, Wu M, Ludwig A, Nitzl G, Tang Y, Hackl G and Watzinger J 2019 *The 8th International SteelSim Conference* SteelSim 2019 (AIST) pp 615–9
[9] Garcia-Hernandez S, Gonzalez-Guzman C H, Morales Davila R, Barreto J de J, Gutierrez E and Calderon-Ramos I 2020 *Crystals* **10** 958
[10] Vakhrushev A, Kharicha A, Wu M, Ludwig A, Nitzl G, Tang Y, Hackl G, Watzinger J and Rodrigues C M G 2020 *IOP Conf. Ser.: Mater. Sci. Eng.* **861** 012015
[11] Wang C, Liu Z and Li B 2021 *Metals* **11** 948
[12] Kharicha A, Vakhrushev A, Karimi-Sibaki E, Wu M and Ludwig A 2021 *Phys. Rev. Fluids* **6** 123701
[13] Vakhrushev A, Kharicha A, Liu Z, Wu M, Ludwig A, Nitzl G, Tang Y, Hackl G and Watzinger J 2020 *Metall. Mater. Trans. B* **51** 2811–28
[14] Vakhrushev A, Kharicha A, Karimi-Sibaki E, Wu M, Ludwig A, Nitzl G, Tang Y, Hackl G, Watzinger J and Eckert S 2021 *Metall. Mater. Trans. B* **52** 3193–207
[15] Vakhrushev A, Karimi-Sibaki E, Bohacek J, Wu M, Ludwig A, Tang Y, Hackl G, Nitzl G, Watzinger J and Kharicha A 2023 *Metals* **13** 444
[16] Torres-Alonso E, Morales R D, Palafox-Ramos J and Ramírez-López P 2008 *Steel Res. Int.* **79** 553–63
[17] Jeon Y J, Sung H J and Lee S 2010 *Metall. Mater. Trans. B* **41** 121–30
[18] Liu Z, Li B and Tsukihashi F 2015 *ISIJ Int.* **55** 805–13
[19] Lu H, Zhong Y, Ren W, Ren Z and Lei Z 2022 *Steel Res. Int.* **93** 2200518
[20] Vakhrushev A, Wu M, Ludwig A, Tang Y, Hackl G and Nitzl G 2014 *Metall. Mater. Trans. B* **45** 1024–37
[21] Nicoud F and Ducros F 1999 *Flow, Turbul. Combust.* **62** 183–200
[22] Ni M-J, Munipalli R, Huang P, Morley N B and Abdou M A 2007 *J. Comput. Phys.* **227** 205–28
[23] Davidson P A 2001 *An Introduction to Magnetohydrodynamics* (Cambridge University Press)
[24] Camporredondo J E, Castillejos A H, Acosta F A, Gutiérrez E P and Herrera M A 2004 *Metall. Mater. Trans. B* **35** 541–60
[25] Vakhrushev A, Kharicha A, Wu M, Ludwig A, Nitzl G, Tang Y, Hackl G, Watzinger J and Rodrigues C M G 2022 *J. Iron Steel Res. Int.* **29** 88–102
[26] Weller H G, Tabor G, Jasak H and Fureby C 1998 *Comput. Phys.* **12** 620
[27] Vakhrushev A, Karimi-Sibaki E, Wu M, Ludwig A, Nitzl G, Tang Y, Hackl G, Watzinger J and Kharicha A 2023 *IOP Conf. Ser.: Mater. Sci. Eng.* **1281** 012026
[28] Miettinen J, Somani M, Visuri V-V, Koskenniska S, Louhenkilpi S, Fabritius T and Kömi J 2022 *Steel Res. Int.* srin.202200120
[29] Zhang H and Wang W 2017 *Metall. Mater. Trans. B* **48** 779–93
[30] Niu Z, Cai Z and Zhu M 2020 *Ironmaking Steelmaking* **47** 1135–47
[31] Vakhrushev A, Karimi-Sibaki E, Wu M, Ludwig A, Nitzl G, Tang Y, Hackl G, Watzinger J, Bohacek J and Kharicha A 2023 *IOP Conf. Ser.: Mater. Sci. Eng.* **1274** 012023
[32] Bohacek J, Kominek J, Vakhrushev A, Karimi-Sibaki E and Lee T 2021 *OpenFOAM J.* **1** 27–46
[33] Vakhrushev A, Kharicha A, Karimi-Sibaki E, Wu M, Ludwig A, Nitzl G, Tang Y, Hackl G and Watzinger J 2022 *Steel Res. Int.* **93** 2200088
[34] Barati H, Wu M, Michelic S, Ilie S, Kharicha A, Ludwig A and Kang Y-B 2021 *Metall. Mater. Trans. B* **52** 4167–78
[35] Vakhrushev A, Kharicha A, Wu M, Ludwig A, Tang Y, Hackl G, Nitzl G, Watzinger J and Bohacek J 2021 *Metals* **11** 1375
[36] Vakhrushev A, Karimi-Sibaki E, Wu M, Ludwig A, Nitzl G, Tang Y, Hackl G, Watzinger J, Bohacek J and Kharicha A 2024 Assessment of URANS-Type Turbulent Flow Modeling of a Single Port Submerged Entry Nozzle (SEN) for Thin Slab Continuous Casting (TSC) Process *Metall. Mater. Trans. B* (*Preprint* 10.1007/s11663-024-03002-8)